

Tunable van Hove singularity without structural instability in Kagome metal CsTi₃Bi₅

Bo Liu^{1,#}, Minquan Kuang^{2,#}, Yang Luo^{1,#}, Yongkai Li^{3,4,#}, Linwei Huai¹, Shuting Peng¹, Zhiyuan Wei¹, Jianchang Shen¹, Bingqian Wang¹, Yu Miao¹, Xiupeng Sun¹, Zhipeng Ou¹, Yugui Yao^{3,4}, Zhiwei Wang^{3,4,5,*} and Junfeng He^{1,*}

¹*Department of Physics and CAS Key Laboratory of Strongly-coupled Quantum Matter Physics, University of Science and Technology of China, Hefei, Anhui 230026, China*

²*Chongqing Key Laboratory of Micro & Nano Structure Optoelectronics, and School of Physical Science and Technology, Southwest University, Chongqing 400715, China*

³*Centre for Quantum Physics, Key Laboratory of Advanced Optoelectronic Quantum Architecture and Measurement (MOE), School of Physics, Beijing Institute of Technology, Beijing 100081, China*

⁴*Beijing Key Lab of Nanophotonics and Ultrafine Optoelectronic Systems, Beijing Institute of Technology, Beijing 100081, China*

⁵*Material Science Center, Yangtze Delta Region Academy of Beijing Institute of Technology, Jiaxing, 314011, China*

[#]These authors contributed equally to this work.

*To whom correspondence should be addressed:

J.H. (jfhe@ustc.edu.cn), Z.W.(zhiweiwang@bit.edu.cn)

In Kagome metal CsV₃Sb₅, multiple intertwined orders are accompanied by both electronic and structural instabilities. These exotic orders have attracted much recent attention, but their origins remain elusive. The newly discovered CsTi₃Bi₅ is a Ti-based Kagome metal to parallel CsV₃Sb₅. Here, we report angle-resolved photoemission experiments and first-principles calculations on pristine and Cs-doped CsTi₃Bi₅ samples. Our results reveal that the van Hove singularity (vHS) in CsTi₃Bi₅ can be tuned in a large energy range without structural instability, different from that in CsV₃Sb₅. As such, CsTi₃Bi₅ provides a complementary platform to disentangle and investigate the electronic instability with a tunable vHS in Kagome metals.

Kagome metals AV_3Sb_5 ($A=K, Rb, Cs$) have attracted much interest due to the coexistence of multiple exotic orders and states, ranging from superconductivity [1-3], charge density wave (CDW) [4-12], pair density wave [12], stripe order [4], nematic order [13,14], topologically nontrivial states [1,15] and time-reversal symmetry breaking states [11,16-18]. Despite the richness of these phenomena, their underlying mechanisms are still under debate. In principle, either electronic or structural instabilities of a material can drive the system into an ordered state with a lower energy. In AV_3Sb_5 ($A=K, Rb, Cs$), electronic instabilities are naturally provided by vHSs in the electron dispersion [19-22], and the structural instabilities are evidenced by the imaginary frequency in the phonon dispersion [23]. As a result, the explanations of the experimentally identified orders are often controversial. For example, the CDW order in AV_3Sb_5 ($A=K, Rb, Cs$) has been attributed to either electronic nesting between van Hove singularities [22-25] or electron-phonon coupling [26-30]; the rotational symmetry breaking has been associated with either electronic nematicity [13] or lattice modulation [14,31]. The coexisted instabilities in both electron and lattice degrees of freedom make it very challenging to identify the primary driving mechanism for the various orders in AV_3Sb_5 ($A=K, Rb, Cs$). In this regard, the importance of comparative studies in a parallel material system is clear. Theoretical calculations have predicted dozens of materials, which are similar to CsV_3Sb_5 [32,33]. However, ATi_3Bi_5 ($A=Cs, Rb$) is the only material family that has been successfully synthesized recently [34,35].

In this paper, we investigate pristine and Cs surface doped $CsTi_3Bi_5$ samples by angle-resolved photoemission spectroscopy (ARPES) and first-principles calculations. The band structure of $CsTi_3Bi_5$ is clearly revealed, which shows a clear resemblance to the calculated results. The vHS is well above Fermi level (E_F) in the pristine $CsTi_3Bi_5$. Surprisingly, the position of the vHS can be easily tuned in a large energy range by Cs surface doping. This property is distinct from that in CsV_3Sb_5 , where the Cs surface doping primarily changes the Sb orbitals but has little effect on the vHS formed by V orbitals. First-principles calculations further reveal the absence of structural instability in both pristine and electron doped $CsTi_3Bi_5$. As such, our results establish $CsTi_3Bi_5$ as a complementary material platform to CsV_3Sb_5 , in which the electronic instability can be systematically examined without the interference from lattice degree of freedom.

Single crystals of $CsTi_3Bi_5$ were grown by a self-flux method with binary Cs-Bi as flux. The raw materials were loaded in an alumina crucible and sealed in an evacuated quartz tube. The tube was

heated slowly to 1000 °C and held for 12 h. It was then cooled down to 850°C at a rate of 10 °C /h and to 500°C at a rate of 3°C /h, at which the flux was removed by a centrifuge. The ARPES measurements were carried out at our lab-based ARPES system using 21.2eV photons with a total energy resolution of ~ 5 meV and a base pressure of better than 5×10^{-11} torr. The Fermi level was determined by measuring a polycrystalline Au piece in electrical contact with the samples. First-principles calculations were performed by using the VASP software package. The details of the calculations and the related parameters are described in the supplemental material.

The crystal structure of CsTi₃Bi₅ is similar to that of CsV₃Sb₅ (Fig. 1a). The Ti sublattice forms a Kagome net, which is interwoven with a hexagonal net of Bi atoms in the same plane. The measured band structure of CsTi₃Bi₅ is shown in Fig. 1b, which bears a clear resemblance to that of the first-principles calculations (Fig. 1d). Due to the layered nature of the material, a projected in-plane Brillouin zone (BZ) is used for the description. The electronic structure near the $\bar{\Gamma}$ point is dominated by an electron-like band (labelled as α band, hereafter), giving rise to a circular Fermi surface sheet (Fig. 1c). Multiple hole-like bands are observed around the \bar{M} point (labelled as β , γ and δ band, respectively). They are associated with the hexagonal, flower-like and diamond-like Fermi surface sheet, respectively (Fig. 1c). A Dirac-like crossing can be seen at \bar{K} , and a triangular Fermi surface sheet is observed around the \bar{K} point (Fig. 1c). The characteristic vHS of the Kagome lattice is shown at \bar{M} point in the calculation (Fig. 1d). Nevertheless, it locates at ~ 150 meV above E_F , which cannot be probed by the photoemission measurements (Fig. 1d).

After revealing the overall electronic structure of the CsTi₃Bi₅, we now investigate the doping evolution via *in situ* surface deposition of Cs atoms. As shown in Fig. 2a, the electron-like band (α band) around $\bar{\Gamma}$ shows a moderate change as a function of Cs doping (Fig. 2a). The distance between the two Fermi momenta (k_{F1} and k_{F2}) increases slightly with doping (Fig. 2b). On the contrary, the energy bands around \bar{M} exhibit more significant changes as a function of Cs doping (Fig. 2d). In particular, the γ and δ bands present a clear downward shift, echoing the expected electron doping with Cs surface deposition. We note that the top of these hole-like bands starts to appear with sufficient Cs doping [Fig. 2d(v)], indicating that the vHS is in the vicinity of E_F . This is also evidenced by the enhanced electron density of states at E_F in this momentum region (Fig. 2e, f). The integrated energy distribution curve (EDC) around the \bar{M} point shows a negligible peak in the pristine CsTi₃Bi₅,

as the vHS is well above E_F (Fig. 2e). However, the peak intensity increases significantly with Cs doping, demonstrating the boost of low energy electron density of states as the vHS approaches E_F (Fig. 2f). In order to quantitatively unveil the vHS, the Cs surface doping is reproduced at an elevated temperature ($T=200K$), where the thermal population of electrons enables a complete examination of the fine features around E_F . As shown in Fig. 3a-d, the vHS is indeed shifted downward with doping. On the sufficiently doped sample, the flat dispersion of the vHS can be clearly identified in the vicinity of E_F (Fig. 3b, d). These results are quantitatively extracted from the data and summarized in Fig. 3f. Orbital-resolved calculations have also been carried out, which illustrate that the electron-like α band around $\bar{\Gamma}$ is dominated by Bi P_z orbital, whereas the vHS is primarily associated with Ti $d_{x^2-y^2}$ orbital (Fig. 3e). These observations have collectively depicted an integrated picture of orbital selective movements of the energy bands with Cs doping -- the vHS with Ti d orbitals can be tuned in a large energy range, whereas the electron-like α band with Bi P orbitals remains less sensitive to the doping process. This is distinct from the evolution in CsV_3Sb_5 , where the vHS with V d orbitals shows little change with Cs surface doping, but the electron-like band with Sb P orbitals shifts ~ 240 meV in energy [36].

Next, we examine the lattice degree of freedom in the $CsTi_3Bi_5$ crystal. We have followed the idea in CsV_3Sb_5 [23], and calculated the change of total energy in $CsTi_3Bi_5$, assuming that the lattice is breathing in and out towards the potential Star of David (SD) and inverse Star of David (ISD) structures (Fig. 4a). In CsV_3Sb_5 , either SD or ISD structure shows a lower total energy than that of the Kagome structure (Fig. 4b), leading to structural instabilities of the material [23]. On the contrary, the Kagome structure in $CsTi_3Bi_5$ exhibits the lowest total energy, demonstrating the absence of structural instability (Fig. 4c). This result remains solid when electron doping is considered in the $CsTi_3Bi_5$ system (Fig. 4d). Phonon spectra are also calculated for both pristine and electron doped $CsTi_3Bi_5$ (Fig. 4e). The absence of imaginary frequency echoes a stable Kagome structure in $CsTi_3Bi_5$.

Finally, we discuss the implications of our observations. The tunable vHS and the absence of structural instabilities make $CsTi_3Bi_5$ a complementary material platform to compare with CsV_3Sb_5 . Without the interference from lattice, one can systematically examine the electronic instabilities associated with the vHS. For example, the CDW order is absent in the pristine $CsTi_3Bi_5$ [34,35], and no CDW gap is observed in our ARPES measurements (see supplemental material). When the vHS is tuned to the vicinity of E_F , the photoemission spectra remain gapless at low temperature (see

supplemental material). These results indicate that the electronic nesting between vHSs at \bar{M} points is insufficient to drive a CDW order in the Kagome metal. The structural instabilities in CsV_3Sb_5 play an essential role in this context. On the other hand, nematic order might be driven by pure electronic interactions, as it has been reported in both CsV_3Sb_5 and CsTi_3Bi_5 [13,14,37,38]. It would be interesting to further explore how the tunable vHS in CsTi_3Bi_5 would interact with the nematic order and other potential electronic orders in the system.

In summary, we have revealed the electronic structure of pristine and Cs surface doped CsTi_3Bi_5 samples. The Cs deposition induces an overall electron doping to the material, but the energy bands exhibit an orbital dependent movement with doping. Among them, the vHS can be tuned in a large energy range. First-principles calculations demonstrate that the Kagome structure remains stable in both pristine and electron doped CsTi_3Bi_5 . These results establish a unique path to disentangle the electronic instability from that of the lattice, and to examine its relationship with the various exotic phenomena in Kagome metals.

- [1] B. R. Ortiz, S. M. L. Teicher, Y. Hu, J. Zuo, P. M. Sarte, E. C. Schueller, A. M. M. Abeykoon, M. J. Krogstad, S. Rosenkranz, R. Osborn, R. Seshadri, L. Balents, J. He, and S. D. Wilson, *Phys. Rev. Lett.* **125**, 247002 (2020).
- [2] B. R. Ortiz, P. M. Sarte, E. M. Kenney, M. J. Graf, S. M. L. Teicher, R. Seshadri, and S. D. Wilson, *Phys. Rev. Mater.* **5**, 034801 (2021).
- [3] Q. Yin, Z. Tu, C. Gong, Y. Fu, S. Yan, and H. Lei, *Chin. Phys. Lett.* **38**, 037403 (2021).
- [4] H. Zhao, H. Li, B. R. Ortiz, S. M. L. Teicher, T. Park, M. Ye, Z. Wang, L. Balents, S. D. Wilson, and I. Zeljkovic, *Nature (London)* **599**, 216-221 (2021).
- [5] Z. Liang, X. Hou, F. Zhang, W. Ma, P. Wu, Z. Zhang, F. Yu, J.-J. Ying, K. Jiang, L. Shan, Z. Wang, and X.-H. Chen, *Phys. Rev. X* **11**, 031026 (2021).
- [6] H. Li, T. T. Zhang, T. Yilmaz, Y. Y. Pai, C. E. Marvinney, A. Said, Q. W. Yin, C. S. Gong, Z. J. Tu, E. Vescovo, C. S. Nelson, R. G. Moore, S. Murakami, H. C. Lei, H. N. Lee, B. J. Lawrie, and H. Miao, *Phys. Rev. X* **11**, 031050 (2021).

- [7] B. R. Ortiz, S. M. L. Teicher, L. Kautzsch, P. M. Sarte, N. Ratcliff, J. Harter, J. P. C. Ruff, R. Seshadri, and S. D. Wilson, *Phys. Rev. X* **11**, 041030 (2021).
- [8] F. H. Yu, D. H. Ma, W. Z. Zhuo, S. Q. Liu, X. K. Wen, B. Lei, J. J. Ying, and X. H. Chen, *Nat. Commun.* **12**, 3645 (2021).
- [9] Y. Song, T. Ying, X. Chen, X. Han, Y. Huang, X. Wu, A.P. Schnyder, J. Guo, and X. Chen, *Phys. Rev. Lett.* **127**, 237001 (2021).
- [10] B. Q. Song, X. M. Kong, W. Xia, Q. W. Yin, C. P. Tu, C. C. Zhao, D. Z. Dai, K. Meng, Z. C. Tao, Z. J. Tu, C. S. Gong, H. C. Lei, Y. F. Guo, X. F. Yang, and S. Y. Li, arXiv:2105.09248 (2021).
- [11] Y.-X. Jiang, J.-X. Yin, M. M. Denner, N. Shumiya, B. R. Ortiz, G. Xu, Z. Guguchia, J. He, M. S. Hossain, X. Liu, J. Ruff, L. Kautzsch, S. S. Zhang, G. Chang, I. Beloposki, Q. Zhang, T. A. Cochran, D. Multer, M. Litskevich, Z.-J. Cheng, X. P. Yang, Z. Wang, R. Thomale, T. Neupert, S. D. Wilson, and M. Z. Hasan, *Nat. Mater.* **20**, 1353-1357 (2021).
- [12] H. Chen, H. Yang, B. Hu, Z. Zhao, J. Yuan, Y. Xing, G. Qian, Z. Huang, G. Li, Y. He, S. Ma, S. Ni, H. Zhang, Q. Yin, C. Gong, Z. Tu, H. Lei, H. Tan, S. Zhou, C. Shen, X. Dong, B. Yan, Z. Wang, and H.-J. Gao, *Nature (London)* **599**, 222-228 (2021).
- [13] L. Nie, K. Sun, W. Ma, D. Song, L. Zheng, Z. Liang, P. Wu, F. Yu, J. Li, M. Shan, D. Zhao, S. Li, B. Kang, Z. Wu, Y. Zhou, K. Liu, Z. Xiang, J. Ying, Z. Wang, T. Wu, and X. Chen, *Nature (London)* **604**, 59-64 (2022).
- [14] Y. Xiang, Q. Li, Y. Li, W. Xie, H. Yang, Z. Wang, Y. Yao, H.-H. Wen, *Nat. Commun.* **12**, 6727 (2021).
- [15] Y. Hu, S. M. L. Teicher, B. R. Ortiz, Y. Luo, S. Peng, L. Huai, J. Ma, N. C. Plumb, S. D. Wilson, J. He, and M. Shi, *Sci. Bull.* **67**, 495 (2022).
- [16] C. M. III, D. Das, J.-X. Yin, H. Liu, R. Gupta, Y.-X. Jiang, M. Medarde, X. Wu, H. C. Lei, J. Chang, P. Dai, Q. Si, H. Miao, R. Thomale, T. Neupert, Y. Shi, R. Khasanov, M. Z. Hasan, H. Luetkens, and Z. Guguchia, *Nature (London)* **602**, 245-250 (2022).

- [17] L. Yu, C. Wang, Y. Zhang, M. Sander, S. Ni, Z. Lu, S. Ma, Z. Wang, Z. Zhao, H. Chen, K. Jiang, Y. Zhang, H. Yang, F. Zhou, X. Dong, S. L. Johnson, M. J. Graf, J. Hu, H. J. Gao, Z. Zhao, arXiv:2107.10741.
- [18] R. Khasanov, D. Das, R. Gupta, C. Mielle, M. Elender, Q. Yin, Z. Tu, C. Gong, H. Lei, E. T. Ritz, R. M. Fernandes, T. Birol, Z. Guguchia, and H. Luetkens, Phys. Rev. Res. **4**, 023224 (2022).
- [19] M. Kang, S. Fang, J.-K. Kim, B. R. Ortiz, S. H. Ryu, J. Kim, J. Yoo, G. Sangiovanni, D. D. Sante, B.-G. Park, C. Jozwiak, A. Bostwick, E. Rotenberg, E. Kaxiras, S. D. Wilson, and J.-H. Park, R. Comin, Nat. Phys. **18**, 301-308 (2022).
- [20] Y. Hu, X. Wu, B. R. Ortiz, S. Ju, X. Han, J. Ma, N. C. Plumb, M. Radovic, R. Thomale, S. D. Wilson, A. P. Schnyder, and M. Shi, Nat. Commun. **13**, 2220 (2022).
- [21] Z. Liu, N. Zhao, Q. Yin, C. Gong, Z. Tu, M. Li, W. Song, Z. Liu, D. Shen, Y. Huang, K. Liu, H. Lei, S. Wang, Phys. Rev. X **11**, 041010 (2021).
- [22] S. Cho, H. Ma, W. Xia, Y. Yang, Z. Liu, Z. Huang, Z. Jiang, X. Lu, J. Liu, Z. Liu, J. Li, J. Wang, Y. Liu, J. Jia, Y. Guo, J. Liu, and D. Shen, Phys. Rev. Lett. **127**, 236401 (2021).
- [23] H. Tan, Y. Liu, Z. Wang, and B. Yan, Phys. Rev. Lett. **127**, 046401 (2021).
- [24] R. Lou, A. Fedorov, Q. Yin, A. Kuibarov, Z. Tu, C. Gong, E.F. Schwier, B. Buchner, H. Lei, and S. Borisenko, Phys. Rev. Lett. **128** 036402 (2022).
- [25] X. Zhou, Y. Li, X. Fan, J. Hao, Y. Dai, Z. Wang, Y. Yao, and H. Wen, Phys. Rev. B **104**, L041101 (2021).
- [26] H. Luo, Q. Gao, H. Liu, Y. Gu, D. Wu, C. Yi, J. Jia, S. Wu, X. Luo, Y. Xu, L. Zhao, Q. Wang, H. Mao, G. Liu, Z. Zhu, Y. Shi, K. Jiang, J. Hu, Z. Xu, and X.J. Zhou, Nat. Commun. **13**, 273 (2022).
- [27] E. Uykur, B. R. Ortiz, S. D. Wilson, M. Dressel, and A. A. Tsirlin, npj Quantum Mater. **7**, 16 (2022).
- [28] Y. Xie, Y. Li, P. Bourges, A. Ivanov, Z. Ye, J. Yin, M.Z. Hasan, A. Luo, Y. Yao, Z. Wang, G. Xu, and P. Dai, Phys. Rev. B **105**, L140501 (2022).

- [29] Z. Ye, A. Luo, J.-X. Yin, M.Z. Hasan, and G. Xu, Phys. Rev. B **105**, 245121 (2022).
- [30] M. Wenzel, B. R. Ortiz, S. D. Wilson, M. Dressel, A. A. Tsirlin, and E. Uyturk, arXiv:211207501 (2021).
- [31] Z. Jiang, H. Ma, W. Xia, Q. Xiao, Z. Liu, Z. Liu, Y. Yang, J. Ding, Z. Huang, J. Liu, Y. Qiao, J. Liu, Y. Peng, S. Cho, Y. Guo, J. Liu, and D. Shen, arXiv:2208.01499 (2022).
- [32] Y. Jiang, Z. Yu, Y. Wang, T. Lu, S. Meng, K. Jiang, and M. Liu, Chin. Phys. Lett. **39**, 047402 (2022).
- [33] X.-W. Yi, X.-Y. Ma, Z. Zhang, Z.-W. Liao, J.-Y. You, G. Su, arXiv:2202.05588 (2022).
- [34] H. Yang, Z. Zhao, X.-W. Yi, J. Liu, J.-Y. You, Y. Zhang, H. Guo, X. Lin, C. Shen, H. Chen, X. Dong, G. Su, H.-J. Gao, arXiv:2209.03840 (2022).
- [35] D. Werhahn, B. R. Ortiz, A. K. Hay, S. D. Wilson, R. Seshadri, S. Johrendt, Zeitschrift für Naturforsch. B online (2022). doi:10.1515/znb-2022-0125.
- [36] K. Nakayama, Y. Li, T. Kato, M. Liu, Z. Wang, T. Takahashi, Y. Yao, and T. Sato, Phys. Rev. X **12**, 011001 (2022).
- [37] H. Yang, Y. Ye, Z. Zhao, J. Liu, X.-W. Yi, Y. Zhang, J. Shi, J. Y. You, Z. Huang, B. Wang, J. Wang, H. Guo, X. Lin, C. Shen, W. Zhou, H. Chen, X. Dong, Z. Wang, H.J. Gao, arXiv:2211.12264 (2022).
- [38] H. Li, S. Cheng, B. R. Ortiz, H. Tan, D. Werhahn, K. Zeng, D. Jorhendt, B. Yan, Z. Wang, S. D. Wilson, I. Zeljkovic, arXiv:2211.16477 (2022).

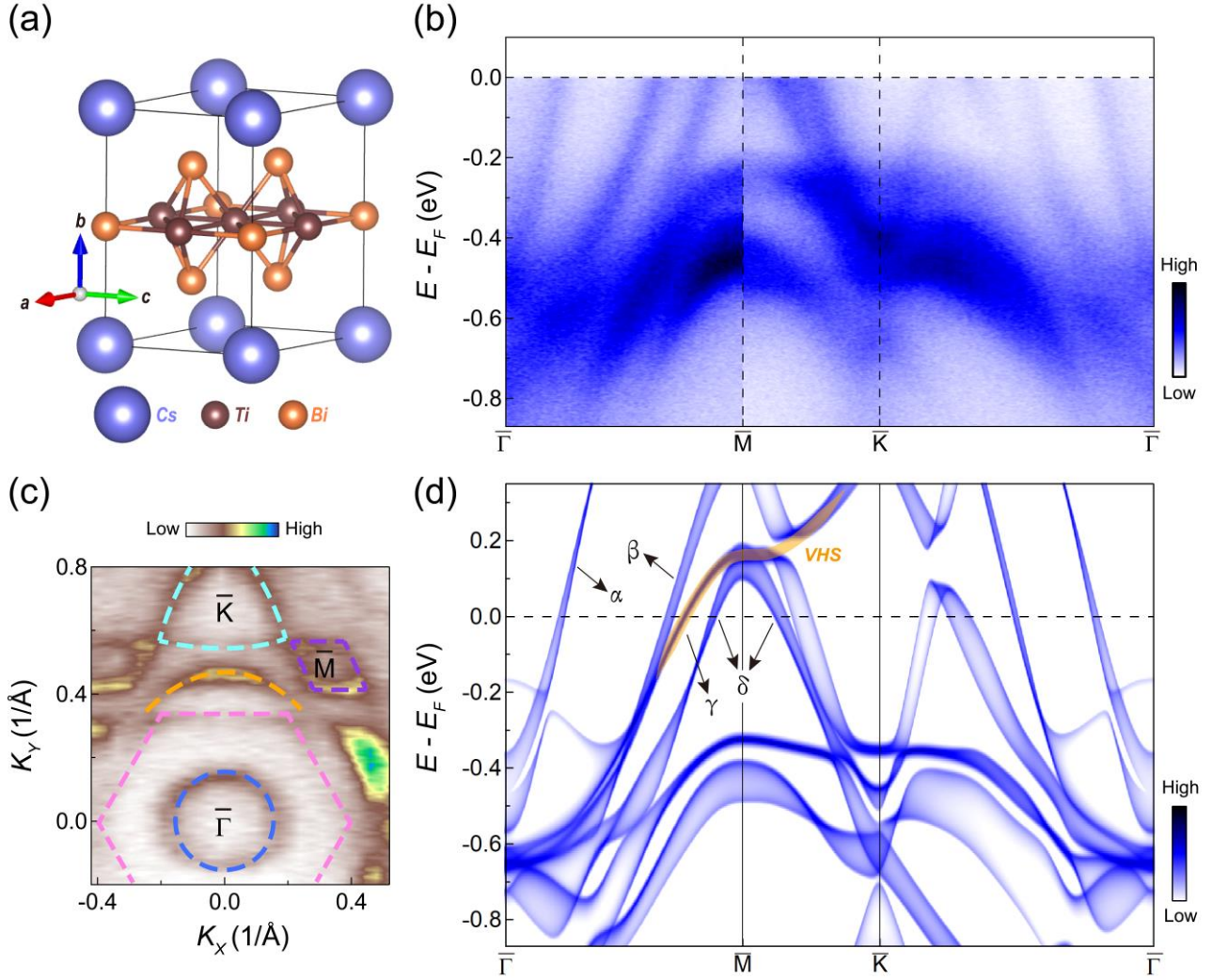


FIG. 1. Electronic structure of CsTi₃Bi₅. (a) Crystal structure of CsTi₃Bi₅. (b-c) Photoelectron intensity plot along $\bar{\Gamma}$ - \bar{M} - \bar{K} - $\bar{\Gamma}$ (b) and Fermi surface (c) of CsTi₃Bi₅ measured with 21.2 eV photons at 7K. The dashed lines in (c) are a guide to the eye. (d) The bulk band structure of CsTi₃Bi₅ obtained from first-principles calculations with spin-orbital coupling included. The electron-like band around $\bar{\Gamma}$ and the hole-like bands near \bar{M} are labelled as α , β , γ and δ band, respectively. The orange shade is an eye-guide for the vHS.

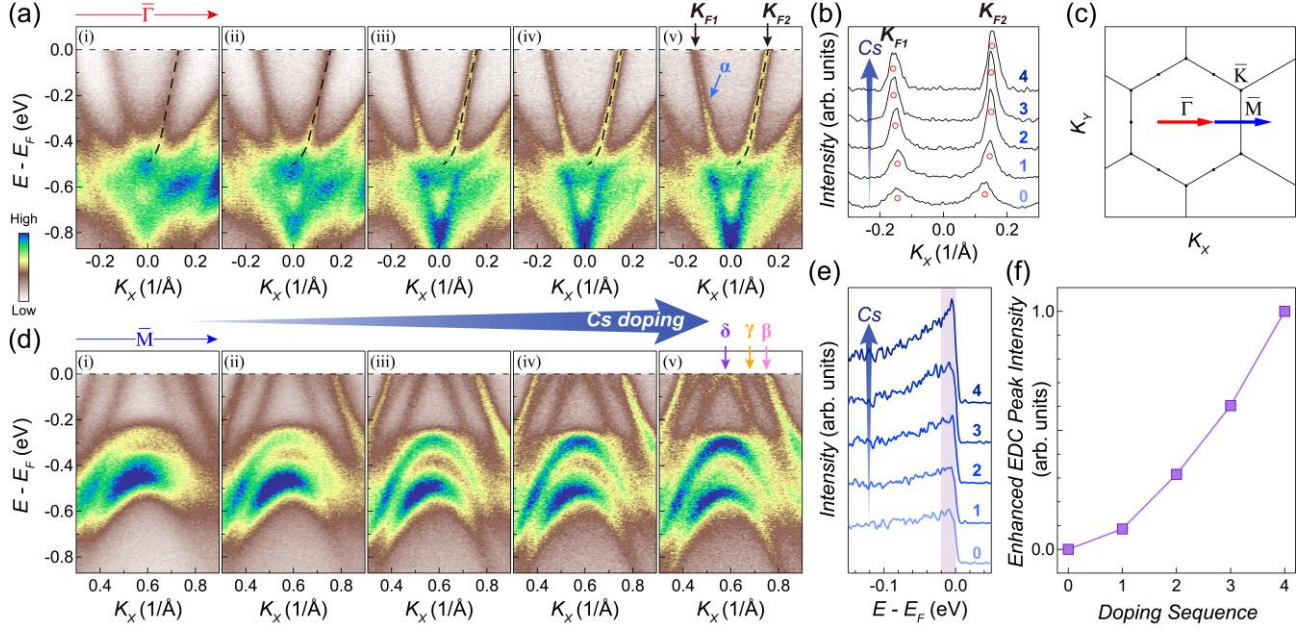


FIG. 2. Evolution of the electronic structure with Cs surface doping at 7K. (a) Photoelectron intensity plot of the band structure around $\bar{\Gamma}$ as a function of continuous Cs doping on the same sample. The results at doping sequences 0-4 are shown in (i-v), respectively. Doping sequence 0 indicates the pristine CsTi_3Bi_5 sample. The dashed lines are a guide to the eye. (b) Momentum distribution curves (MDCs) at E_F extracted from (a). (c) The projected in-plane BZ and the momentum locations of the cuts. (d) Same as (a), but for the band structure around \bar{M} . (e) Integrated EDC around the \bar{M} point in (d). The numbers 0-4 denote the doping sequences. (f) Enhanced EDC peak intensity around \bar{M} as a function of the doping sequence. The absolute EDC peak intensity at the doping sequence x ($x=0-4$) is calculated by integrating the area between -20meV and E_F of the corresponding EDC, and labelled as I_x . The enhanced EDC peak intensity is defined as $(I_x - I_0)/(I_4 - I_0)$.

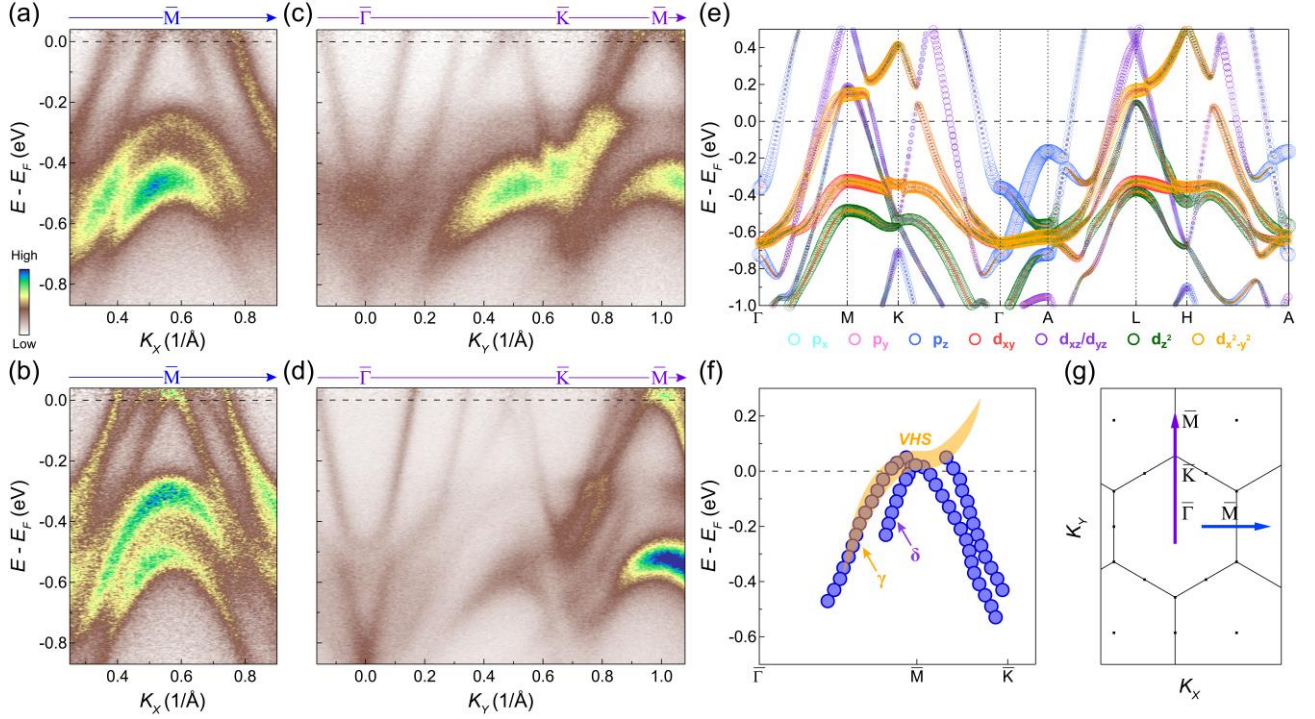


FIG. 3. Doping evolution of the vHS. (a-b) Photoelectron intensity plot of the band structure around \bar{M} (along the $\bar{\Gamma}-\bar{M}-\bar{\Gamma}$ direction) before (a) and after (b) the Cs surface doping, measured at 200K. (c-d) Same as (a-b), but measured along the $\bar{\Gamma}-\bar{K}-\bar{M}$ direction. (e) Orbital-resolved band structure obtained by first-principles calculations. (f) Quantified dispersion of the γ and δ bands near \bar{M} after sufficient Cs doping, extracted from (b) and (d). The orange shade is an eye-guide for the vHS. (g) Momentum locations of the cuts in the BZ.

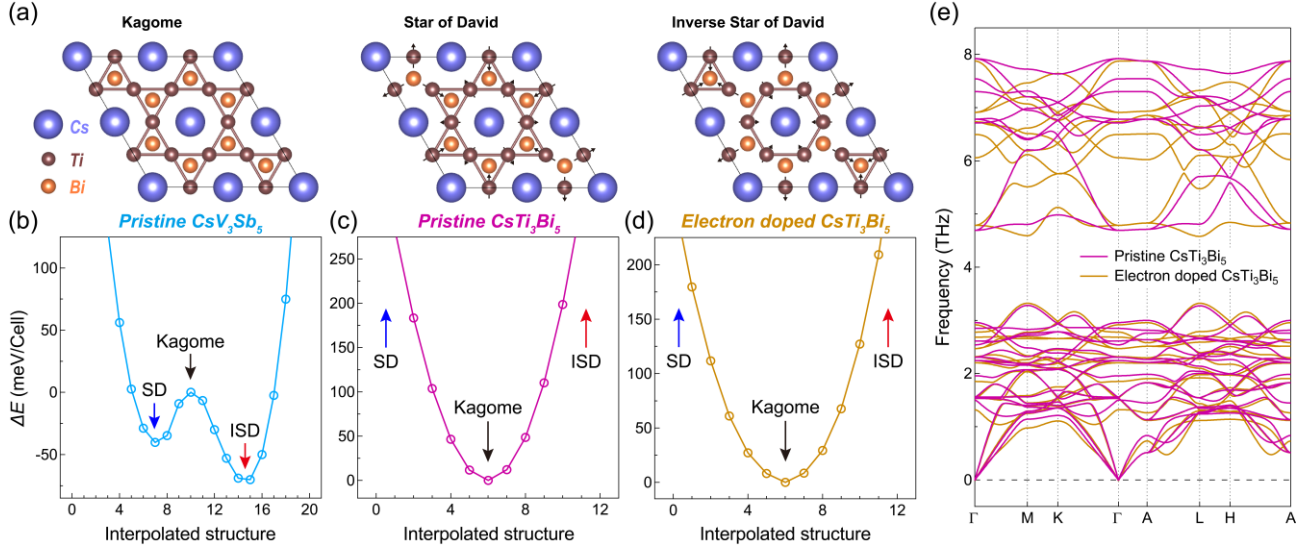


FIG. 4. Calculated total energy profiles and phonon spectra. (a) The 2x2 supercells for Kagome structure, Star of David structure and Inverse Star of David structure. The black arrows indicate the lattice distortion due to the breathing mode. (b-d) Total energy as a function of the interpolated structure in pristine CsV_3Sb_5 (b), pristine CsTi_3Bi_5 (c), and electron doped CsTi_3Bi_5 (d). (e) Calculated phonon spectra along the high-symmetry directions in pristine CsTi_3Bi_5 (magenta line) and electron doped CsTi_3Bi_5 (orange line).